JOURNAL OF THERMOPHYSICS AND HEAT TRANSFER
Vol. 23, No. 4, October–December 2009

Cylindrical Geometry Verification Problem for Enclosure Radiation

Ben Blackwell*
Blackwell Consulting, Corrales, New Mexico 87048
Kevin Dowding†
Sandia National Laboratories, Albuquerque, New Mexico 87185
and
Michael Modest‡
Pennsylvania State University, University Park, Pennsylvania 16802

DOI: 10.2514/1.39861

The development of a manufactured solution for enclosure radiation in an infinitely long circular cylinder with a nonparticipating medium is presented. This solution is then used to verify the correct implementation of the commonly used discrete enclosure equations. The circular cross section is approximated by a faceted geometry; the numbers of facets used are 4, 8, 16, 32, 64, and 128. The crossed-string method, which is exact in this application, is used to compute the view factors. Computational results using six levels of grid refinement suggest that the error norm between the integral equation solution and the discrete equation solution behaves as h^2 where h is a characteristic mesh size.

Nomenclature

A, A'	=	surface area, m^2, also region A
B, B_1, B_2	=	region identifiers
a, b	=	integration limits
C, C_1, C_2	=	constants
E_b	=	blackbody emissive power, W/m^2
E_{b_o}	=	blackbody emissive power evaluate at T_o, W/m^2; see Eq. (15)
e	=	error in numerical solution
F	=	view factor, dimensionless
F_{ij}	=	view factor between surfaces i and j, dimensionless
$f(x)$	=	function of x
H	=	irradiation, W/m^2
H'	=	dimensionless irradiation; see Eq. (25)
h	=	characteristic mesh size, m
i	=	position index
J	=	radiosity, W/m^2
J'	=	dimensionless radiosity; see Eq. (24)
K	=	kernel, $1/m^2$; see Eq. (6)
k	=	integer
$L_2(e)$	=	$(\sum_{i=1}^{N} \lvert e_i \rvert^2)^{\frac{1}{2}}$
N	=	number of surface facets
p	=	order of grid convergence
q	=	heat flux, W/m^2
q'	=	dimensionless heat flux, see Eq. (26)
r	=	radius of cylinder, m
$\mathbf{r}_i$, $\mathbf{r}_j$	=	position vector on surface i or j
S	=	distance between surface elements, m
s	=	arc length, m
T	=	temperature, K
T_i	=	temperature of facet i, K
T_o	=	enclosure temperature at $\theta = 0$, K
T'	=	dimensionless temperature; see Eq. (27)
x_0, x_1	=	integration limits; see Eq. (30)
α	=	angle, deg
β	=	angle, deg
ϵ	=	emittance
θ, θ'	=	angle, deg
ξ	=	a value in the interval $a < \xi < b$; see Eqs. (30) and (31)
ρ	=	reflectance
σ	=	Stefan–Boltzmann constant, $W/m^2 \cdot K^4$

Received 18 July 2008; revision received 30 March 2009; accepted for publication 26 May 2009.

*President, Post Office Box 2879. Associate Fellow AIAA.
†Technical Staff Member, Mail Stop 0828. Senior Member AIAA.
‡Distinguished Professor, 301C Reber Building. Associate Fellow AIAA.

I. Introduction

MODERN computational software may contain tens to hundreds of thousands of lines of code. To develop confidence that there are no coding mistakes, a formal code verification process should be an integral part of the code development process. For the purposes of this paper, code verification is the *process of ensuring that the model equations are implemented and solved correctly.* The ideal time for code verification is while the software is being developed. All code development teams do some amount of code verification during the development process. Unfortunately, the end user of the software may not have access to this information. If, for example, one models mission critical components that may get too hot or have stress levels that are too high, then the end user should do some code verification.

Significant strides have been made in the code verification arena. Books with "verification" in the title are starting to appear (Roache [1] and Knupp and Salari [2]) as the technology matures. The most commonly used approach for code verification involving ordinary and partial differential equations as well as integral equations is the *order verification procedure*. If h is a characteristic mesh size, the discretization error e in the numerical solution behaves as h^p, where p is the order of convergence. Mathematically, this can be expressed as

$$e = Ch^p + \text{HOT} \tag{1}$$

where C is a constant, and HOT refers to higher-order terms. A sequence of meshes is used to estimate p from the errors in the numerical results. If the computed p does not match the theoretical p, then there can be errors other than discretization errors or there

are higher-order terms present in Eq. (1) (not in asymptotic range). The analytical solution used in the verification process can be obtained from either classical methods (separation of variables, Green's functions, etc.) or the method of manufactured solutions [1,2].

Few analytical solutions exist for the integral equations that describe enclosure radiation with a nonparticipating medium. Sparrow [3] developed a solution for a semicircular cylindrical surface of infinite length. Modest [4] presented a solution for a partial enclosure of a circular cross section with a line source located along the axis. The works of Sparrow [3] and Modest [4] will be used to guide the development of an analytical solution (manufactured solution) for a cylindrical cross-sectional enclosure of infinite length; no external irradiation or energy sources are present. This solution will be used as a verification problem for the discrete surface with a uniform radiosity approximation to the integral equations.

II. Presentation of Integral Equations for Enclosure Radiation

The radiosity (J), irradiation (H), and net heat flux (q) notation of Modest [4] will be used. The radiosity is the radiant flux leaving a surface at position $\mathbf{r}_i$, is composed of an emitted component and a reflected component, and is given by

$$J_i(\mathbf{r}_i) = \epsilon_i E_{b_i}(\mathbf{r}_i) + \rho_i H_i(\mathbf{r}_i) \tag{2}$$

where E_{b_i} is the blackbody emissive power given by

$$E_{b_i}(\mathbf{r}_i) = \sigma T_i^4(\mathbf{r}_i) \tag{3}$$

and H_i is the irradiation for surface i. For a gray surface (emittance = absorptance), the radiosity equation becomes

$$J_i(\mathbf{r}_i) = \epsilon_i \sigma T_i^4(\mathbf{r}_i) + (1-\epsilon_i) H_i(\mathbf{r}_i) \tag{4}$$

The irradiation of surface i is composed of the radiant flux leaving all surfaces of the enclosure and is given by

$$H_i(\mathbf{r}_i) = \sum_{j=1}^{N} \int_{A_j} J_j(\mathbf{r}_j)\, \mathrm{d}F_{dA_i - dA_j} = \sum_{j=1}^{N} \int_{A_j} J_j(\mathbf{r}_j) K(\mathbf{r}_i, \mathbf{r}_j)\, \mathrm{d}A_j \tag{5}$$

where the geometric view factor is defined by

$$dA_i dF_{dA_i - dA_j} = dA_j dF_{dA_j - dA_i} = \frac{\cos\theta_i \cos\theta_j}{\pi S^2}$$

with θ_i being the angle between the surface normal and the line connecting the surfaces that are a distance S apart. The kernel function K is defined by

$$K(\mathbf{r}_i, \mathbf{r}_j) = \frac{\mathrm{d}F_{dA_i - dA_j}}{\mathrm{d}A_j} = \frac{\mathrm{d}F_{dA_j - dA_i}}{\mathrm{d}A_i} \tag{6}$$

The final expression for the integral equation describing the radiosity distribution is given by

$$J_i(\mathbf{r}_i) = \epsilon_i \sigma T_i^4(\mathbf{r}_i) + (1-\epsilon_i) \sum_{j=1}^{N} \int_{A_j} J_j(\mathbf{r}_j) K(\mathbf{r}_i, \mathbf{r}_j)\, \mathrm{d}A_j \qquad 1 \le i \le N \tag{7}$$

If the temperature distribution is specified, then Eq. (7) is a system of N linear (for the case of radiant properties independent of temperature) integral equations in the unknown radiosity for the N surfaces.

III. Analytical Solution to Integral Form of Radiosity Equations

Modest [4] presented the analytical solution for a hollow cylindrical enclosure of infinite length with an opening in the side and a line source located along the cylindrical axis. The work of Modest [4] will be the starting point for the development of our verification problem. In this work, the cross section is a full 360 deg enclosure and there are no sources present. In Figs. 5–16 of Modest [4], our problem corresponds to an opening angle and line source of zero ($\varphi = 0$ and $Q' = 0$ in the notation of Modest [4]). The integral equation that the radiosity must satisfy reduces to

$$J(\theta) = \epsilon\sigma T^4(\theta) + (1-\epsilon) \int_{A'} J(\theta')\, \mathrm{d}F_{dA - dA'} \tag{8}$$

The view factor between two differential elements on the surface of the cylinder is given by ([4,5] or [6])

$$dF_{dA-dA'} = d(\sin\beta) = \tfrac{1}{2}\cos\beta d\beta \tag{9}$$

where $0 \le \beta \le \pi/2$ is the angle between the surface normal and the line connecting the differential elements; see Fig. 1 for details. Let θ be the angular position of surface element dA and θ' be the angular position of surface element dA'; both θ and θ' are measured counterclockwise from the south pole of the cross section and are restricted to the range $-\pi$ to π. The angle $0 \le \alpha \le \pi$ is the angle defined by the θ and θ' rays. From elementary trigonometry,

$$\alpha + 2\beta = \pi \tag{10}$$

The angle α will have three different definitions depending on where on the circle dA' is located. Divide the circle into two halves using a line through the origin and dA; the region below this line will be designated region A. Because β is in the range of $0 \le \beta \le \pi/2$, the limits of integration in Eq. (8) must be chosen carefully so that all integrals have $d\beta > 0$. From the information given in Fig. 1, it is possible to derive the results given in Table 1. These results are useful in the derivations that follow.

The region above the dividing line in Fig. 1 will be denoted by region B. This region must be further subdivided into two regions because of the constraint $-\pi \le \theta' \le \pi$. These two regions are shown in Fig. 2. From the information given in Fig. 2, it is possible to derive the results given in Table 2.

To confirm the geometry results already given, the view factor $F_{dA-A'}$ will be computed; the results are known to be unity.

$$F_{dA-A'} = -\frac{1}{4}\int_{\theta-\pi}^{\theta} \sin\left(\frac{\theta'-\theta}{2}\right) \mathrm{d}\theta' + \frac{1}{4}\int_{\theta-\pi}^{-\pi} \sin\left(\frac{\theta'-\theta}{2}\right) \mathrm{d}\theta' - \frac{1}{4}\int_{\pi}^{\theta} \sin\left(\frac{\theta'-\theta}{2}\right) \mathrm{d}\theta'$$

The first two integrals can be combined and the limits interchanged on the third integral, yielding

$$F_{dA-A'} = -\frac{1}{4}\int_{-\pi}^{\theta} \sin\left(\frac{\theta'-\theta}{2}\right) \mathrm{d}\theta' + \frac{1}{4}\int_{\theta}^{\pi} \sin\left(\frac{\theta'-\theta}{2}\right) \mathrm{d}\theta' = 1$$

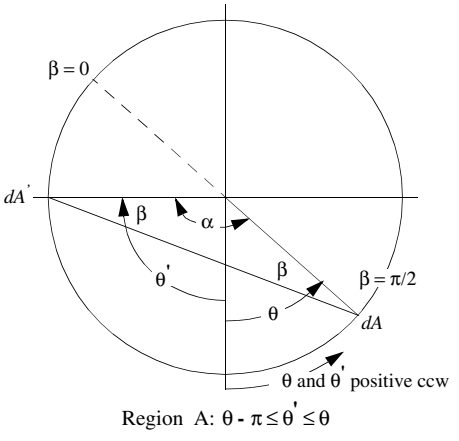

Region A: $\theta - \pi \le \theta' \le \theta$

Fig. 1 Geometry for circular cross-sectional enclosure for region A.

Table 1 Geometry information for region A

Region A: $\theta-\pi\le\theta'\le\theta$
$0\le\alpha=-(\theta'-\theta)\le\pi$
$\beta=\frac{\pi}{2}+\frac{\theta'-\theta}{2}>0$
$d\beta=\frac{d\theta'}{2}$
$\cos(\beta)=-\sin\frac{1}{2}(\theta'-\theta)$
$dF_{dA-dA'}=-\frac{1}{4}\sin\frac{1}{2}(\theta'-\theta)d\theta'$
$0\le\beta\le\pi/2$
$\theta-\pi\ge\theta'\ge\theta$

Table 2 Geometry information for region B

Region B_1: $-\pi\le\theta'<\theta-\pi$	Case B_2: $\theta\le\theta'<\pi$
$0\le\alpha=2\pi+(\theta'-\theta)\le\pi$	$0\le\alpha=\theta'-\theta\le\pi$
$\beta=-\frac{\pi}{2}-\frac{\theta'-\theta}{2}>0$	$\beta=(\pi/2)-(\theta'-\theta/2)>0$
$d\beta=-\frac{d\theta'}{2}$	$d\beta=-(d\theta'/2)$
$\cos(\beta)=-\sin\frac{1}{2}(\theta'-\theta)$	$\cos(\beta)=\sin\frac{1}{2}(\theta'-\theta)$
$dF_{dA-dA'}=\frac{1}{4}\sin\frac{1}{2}(\theta'-\theta)d\theta'$	$dF_{dA-dA'}=-\frac{1}{4}\sin\frac{1}{2}(\theta'-\theta)d\theta'$
$0\le\beta\le\theta/2$	$\theta/2\le\beta\le\pi/2$
$\theta-\pi\ge\theta'\ge-\pi$	$\pi\ge\theta'\ge\theta$

This result confirms the validity of the geometry information used so far in the analysis.

The integral equation describing the radiosity distribution can now be written as

$$J(\theta)=\epsilon\sigma T^4(\theta)-\frac{1-\epsilon}{4}\int_{-\pi}^{\theta}J(\theta')\sin\left(\frac{\theta'-\theta}{2}\right)\mathrm{d}\theta'+\frac{1-\epsilon}{4}\int_{\theta}^{\pi}J(\theta')\sin\left(\frac{\theta'-\theta}{2}\right)\mathrm{d}\theta' \tag{11}$$

Following Sparrow [3] and Modest [4], Eq. (11) can be converted to a differential equation by double differentiation with respect to θ. Using Leibnitz's rule, we have

$$\frac{dJ(\theta)}{d\theta}=\epsilon\frac{dE_b}{d\theta}-\frac{1-\epsilon}{4}\left(-\frac{1}{2}\right)\int_{-\pi}^{\theta}J(\theta')\cos\left(\frac{\theta'-\theta}{2}\right)\mathrm{d}\theta'+\frac{1-\epsilon}{4}\left(-\frac{1}{2}\right)\int_{\theta}^{\pi}J(\theta')\cos\left(\frac{\theta'-\theta}{2}\right)\mathrm{d}\theta' \tag{12}$$

$$\frac{d^2J}{d\theta^2}=\epsilon\frac{d^2E_b}{d\theta^2}+\frac{1-\epsilon}{4}J(\theta)-\frac{1}{4}\left[-\frac{1-\epsilon}{4}\int_{-\pi}^{\theta}J(\theta')\sin\left(\frac{\theta'-\theta}{2}\right)\mathrm{d}\theta'+\frac{1-\epsilon}{4}\int_{\theta}^{\pi}J(\theta')\sin\left(\frac{\theta'-\theta}{2}\right)\mathrm{d}\theta'\right] \tag{13}$$

From Eq. (11) it follows that the term inside the square brackets in Eq. (13) is equal to $J(\theta)-\epsilon E_b$. The final result is

$$\frac{d^2J}{d\theta^2}+\frac{\epsilon}{4}J=\epsilon\left(\frac{d^2E_b}{d\theta^2}+\frac{1}{4}E_b\right) \tag{14}$$

Because we are developing a manufactured solution for a verification problem, we are free to choose E_b based on convenience. If we choose

$$E_b(\theta)=E_{b_o}\cos(\theta/2)$$
$$E_{b_o}=\sigma T_o^4\quad\text{or}\quad T(\theta)=T_o(\cos(\theta/2))^{\frac{1}{4}} \tag{15}$$

then the right-hand side of Eq. (14) is identically zero. Note that E_b is symmetric about $\theta=0$ and is positive for $-\pi\le\theta\le\pi$; the temperature is a maximum at the south pole and zero at the north pole. The solution of the resulting homogeneous second-order ode for J, Eq. (14), is

$$J(\theta)=C_1\sin\left(\frac{\sqrt{\epsilon}}{2}\theta\right)+C_2\cos\left(\frac{\sqrt{\epsilon}}{2}\theta\right)$$

Following Modest [4], we will use symmetry to determine C_1. Because E_b is symmetric about $\theta=0$, it is reasonable to stipulate that $J(\theta)=J(-\theta)$; this forces $C_1=0$. The resulting analytical solution for the radiosity distribution is

$$J(\theta)=C_2\cos((\sqrt{\epsilon}/2)\theta) \tag{16}$$

The constant C_2 will be determined from $J(\theta)|_{\theta=0}$. From Eq. (11), we have

$$J(0)=\epsilon E_b(0)-\frac{1-\epsilon}{4}\int_{-\pi}^{0}J(\theta')\sin\left(\frac{\theta'}{2}\right)\mathrm{d}\theta'+\frac{1-\epsilon}{4}\int_{\theta}^{\pi}J(\theta')\sin\left(\frac{\theta'}{2}\right)\mathrm{d}\theta' \tag{17}$$

Substituting Eq. (16) into Eq. (17) yields

$$C_2=\epsilon E_b(0)+C_2\frac{1-\epsilon}{4}\left[-\int_{-\pi}^{0}\cos\left(\frac{\sqrt{\epsilon}}{2}\theta'\right)\sin\left(\frac{\theta'}{2}\right)\mathrm{d}\theta'+\int_{0}^{\pi}\cos\left(\frac{\sqrt{\epsilon}}{2}\theta'\right)\sin\left(\frac{\theta'}{2}\right)\mathrm{d}\theta'\right]$$

Through a change of variable, the first integral can be made to look like the second integral, resulting in

$$C_2=\epsilon E_{b_o}+C_2\frac{1-\epsilon}{4}2\int_{0}^{\pi}\cos\left(\frac{\sqrt{\epsilon}}{2}\theta'\right)\sin\left(\frac{\theta'}{2}\right)\mathrm{d}\theta'$$

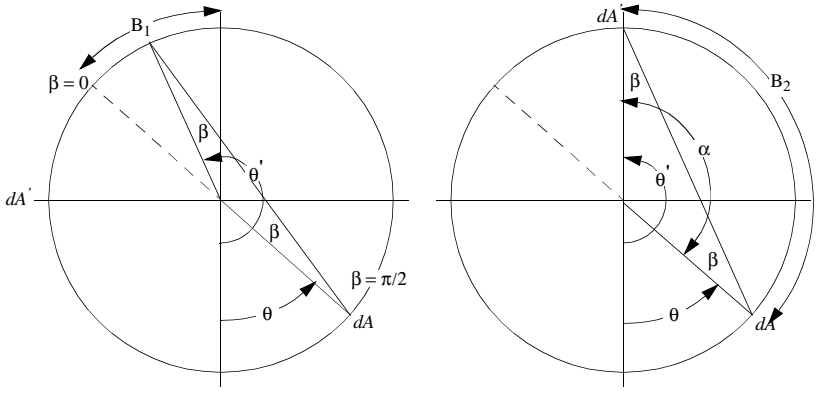

Region B_1: $-\pi\le\theta'\le\theta-\pi$ Region B_2: $\theta\le\theta'\le\pi$

Fig. 2 Geometry for circular cross-sectional enclosure with regions B_1 and B_2 identified.

Evaluating the integrals and solving for C_2 yields

$$C_2 = \frac{\epsilon E_{b_o}}{\sqrt{\epsilon}\sin(\sqrt{\epsilon}/2)\pi}$$

Note that for a blackbody, $C_2 = E_{b_o}$. The final solution for the radiosity distribution is

$$J(\theta) = \frac{\sqrt{\epsilon}E_{b_o}}{\sin(\sqrt{\epsilon}/2)\pi}\cos((\sqrt{\epsilon}/2)\theta) \tag{18}$$

Knowing the radiosity distribution, both the irradiation (H) and heat flux (q) distributions can be calculated. From Modest [4], the heat flux is the difference between the radiosity and irradiation:

$$q(\theta) = J(\theta) - H(\theta) \tag{19}$$

where the irradiation is related to the radiosity by

$$H(\theta) = \int_{A'} J(\theta')\,\mathrm{d}F_{dA-dA'} \tag{20}$$

The irradiation can be extracted from Eq. (11) and is

$$H(\theta) = -\frac{1}{4}\int_{-\pi}^{\theta} J(\theta')\sin\left(\frac{\theta'-\theta}{2}\right)\mathrm{d}\theta' + \frac{1}{4}\int_{\theta}^{\pi} J(\theta')\sin\left(\frac{\theta'-\theta}{2}\right)\mathrm{d}\theta' \tag{21}$$

Substituting Eq. (18) into Eq. (21) yields

$$H(\theta) = \frac{1}{4}\frac{\sqrt{\epsilon}E_{b_o}}{\sin(\sqrt{\epsilon}/2)\pi}\left[-\int_{-\pi}^{\theta}\cos\left(\frac{\sqrt{\epsilon}}{2}\theta\right)\sin\left(\frac{\theta'-\theta}{2}\right)\mathrm{d}\theta' + \int_{\theta}^{\pi}\cos\left(\frac{\sqrt{\epsilon}}{2}\theta\right)\sin\left(\frac{\theta'-\theta}{2}\right)\mathrm{d}\theta'\right]$$

Performing the indicated integration yields

$$H(\theta) = \frac{\sqrt{\epsilon}}{1-\epsilon}E_{b_o}\left(\frac{\cos((\sqrt{\epsilon}/2)\theta)}{\sin(\sqrt{\epsilon}/2)\pi} - \sqrt{\epsilon}\cos(\theta/2)\right) \tag{22}$$

Using Eq. (19), the heat flux becomes

$$q(\theta) = \frac{\epsilon}{1-\epsilon}E_{b_o}\left[\cos(\theta/2) - \sqrt{\epsilon}\frac{\cos((\sqrt{\epsilon}/2)\theta)}{\sin(\sqrt{\epsilon}/2)\pi}\right] \tag{23}$$

If J, H, and q are normalized by E_{b_o}, the results are dimensionless and depend only on ϵ and θ. The resulting dimensionless quantities are

$$J' = \frac{J}{E_{b_o}} = \frac{\sqrt{\epsilon}}{\sin(\sqrt{\epsilon}/2)\pi}\cos((\sqrt{\epsilon}/2)\theta) \tag{24}$$

$$H' = \frac{H}{E_{b_o}} = \frac{\sqrt{\epsilon}}{1-\epsilon}\left(\frac{\cos((\sqrt{\epsilon}/2)\theta)}{\sin(\sqrt{\epsilon}/2)\pi} - \sqrt{\epsilon}\cos(\theta/2)\right) \tag{25}$$

$$q' = \frac{q}{E_{b_o}} = \frac{\epsilon}{1-\epsilon}\left[\cos(\theta/2) - \sqrt{\epsilon}\frac{\cos((\sqrt{\epsilon}/2)\theta)}{\sin(\sqrt{\epsilon}/2)\pi}\right] \tag{26}$$

$$T' = (T/T_o) = (\cos(\theta/2))^{\frac{1}{4}} \tag{27}$$

where T' is the dimensionless temperature; note that the temperature at the top ($\theta = \pi$) is absolute zero. These equations are displayed graphically in Fig. 3 for $\epsilon = 0.9$. Note that the results are symmetric about $\theta = 0$. Heat is leaving the bottom of the enclosure ($J > H$) and flows into the top of the enclosure ($J < H$).

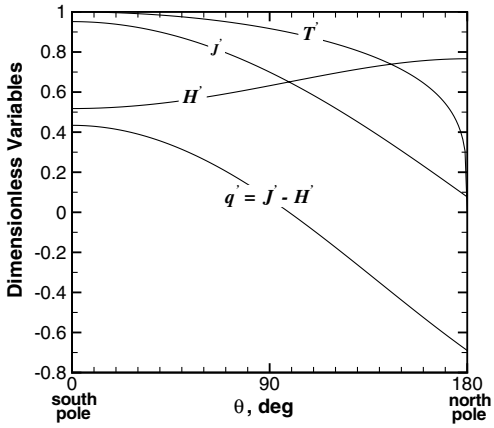

Fig. 3 Results for cylindrical cross-sectional enclosure with $\epsilon = 0.9$.

IV. Discrete Enclosure Equations and Their Solution

The discrete form of the enclosure equations is obtained from the integral form by assuming the radiosity is uniform over each faceted surface. This allows the unknown radiosity to be brought outside the integral sign and naturally introduces the definition of the view factor. This approach is similar to using the midpoint rule to evaluate an integral with the exception that the remaining kernel is integrated properly. From Modest [4], these equations are

$$J_i - (1-\epsilon_i)\sum_{j=1}^{N} J_j F_{i-j} = \epsilon_i \sigma T_i^4 \tag{28}$$

$$q_i = (\epsilon_i/(1-\epsilon_i))(\sigma T_i^4 - J_i) = J_i - H_i \tag{29}$$

Although there are other discrete approximations to Eq. (7), Eq. (28) is a commonly implemented form. These discrete equations are linear in J_i for radiative properties independent of temperature.

It is desirable to know the theoretical order of convergence (p) of the discretization error (Eq. (1)) as the grid in Eq. (28) is refined. In the present problem, as in many practical nonlinear problems, the analysis for theoretical p is neither straightforward nor unique.[§] The absence of a theoretical p should not be used as an excuse for not performing a grid refinement study. In this instance, theoretical results from the discretization error for the midpoint integration rule will be used to guide the discussion about the theoretical p for this problem. Mathews [7] presented the result

$$\int_{x_o}^{x_1} f(x)\,\mathrm{d}x = hf\left(x_o + \frac{h}{2}\right) + \frac{h^3}{24}f''(\xi) \quad \text{where } h = x_1 - x_o \quad \text{and} \quad x_o < \xi < x_1 \tag{30}$$

which indicates that the discretization error for the single interval midpoint rule is $\mathcal{O}(h^3)$. However, the composite midpoint rule [7] has a discretization error given by

$$\int_a^b f(x)\,\mathrm{d}x = h\sum_{k=1}^{N} f\left(a + \left(k - \frac{1}{2}\right)h\right) + \frac{(b-a)}{24}h^2 f''(\xi) \quad \text{where } h = \frac{b-a}{N} \tag{31}$$

where N is the number of subintervals. Because Eq. (28) was derived from Eq. (7) using something more akin to the composite midpoint rule, it is argued that the discretization error for Eq. (28) is likely to be $\mathcal{O}(h^2)$ instead of $\mathcal{O}(h^3)$. A rigorous proof is needed to conclusively demonstrate the theoretical order of convergence. Regardless, our numerical results will provide the actual order of convergence for this case.

[§]Roache, P. J., private communication, 2008.

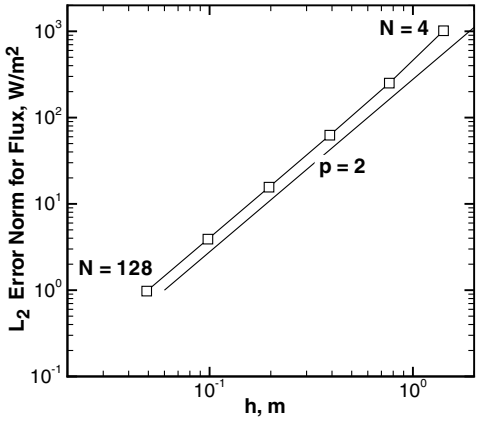

Fig. 4 Heat flux grid convergence results for radiation in a circular enclosure: $\epsilon = 0.9$ and $T_o = 1000$ K.

The geometry for the discrete equations is an approximation to the circular cross section. In effect, a circular arc s is approximated by its chord h. The geometry error in approximating a circular arc by its chord is

$$s - h = \tfrac{1}{6}(h^3/(2r)^2) + \mathcal{O}(h^5) \tag{32}$$

Consequently, it is argued that the grid errors introduced by solving the discrete equations on a changing geometry will be smaller than the discretization errors associated with Eq. (28).

The view factors for the faceted geometry were computed using Hottel's crossed-strings method [4]. This method is exact for the faceted geometry of this problem.

V. Computational Results

Results were computed on a sequence of faceted approximations to the circular geometry. The number of facets used was 4, 8, 16, 32, 64, and 128. The computational sequence was as follows:

1) Divide the circular geometry into N uniform facets of size h with nodes at the north and south poles.

2) Using the analytical solution, compute the temperature of the facet at the angle θ corresponding to the facet midpoint.

3) Compute the facet radiosity from Eq. (28).

4) Compute the facet heat flux from Eq. (29).

5) Compute the error in facet heat flux by comparing it with the analytical solution for the heat flux, Eq. (26).

6) Repeat steps 1–5 for the next value of N.

Results for this sequence of computations are given in Fig. 4. With the exception of the coarsest grid, the L_2 heat flux error norm results follow the $p = 2$ line very closely. This type of analysis depends on being in the "asymptotic range," which simply means that the leading term in a Taylor series is dominant. When a circle is approximated by a square ($N = 4$), the discrete geometry is a crude approximation to the actual geometry. It is not surprising that the $N = 4$ results are not in the asymptotic range.

VI. Conclusions

An analytical solution was developed for enclosure radiation in a two-dimensional circular cylinder. The problem was motivated by the desire to perform code verification involving enclosure radiation. The analytical solution is not for a physically real problem, but code verification is only concerned with mathematics and its correct implementation. The argument presented for the theoretical order of convergence of the discrete form of the enclosure equations is not rigorous. However, the computational results appear to follow the second-order convergence line very closely. Our experience (as well as that of [1,2]) with the order verification procedure is that the method is very sensitive to detecting code bugs and/or input errors. The computational results lead us to believe that the discrete form of the radiosity equations has a second-order truncation error and that we have verified our implementation of the method.

Acknowledgments

This work was supported by Sandia National Laboratories, a multiprogram laboratory operated by Sandia Corporation, a Lockheed Martin Company, for the U.S. Department of Energy's National Nuclear Security Administration under contract DE-AC04-94AL85000. The authors acknowledge discussions with Ron Dykhuizen of Sandia National Laboratories that improved the clarity of the paper.

References

[1] Roache, P. J., *Verification and Validation in Computational Science and Engineering*, Hermosa, Albuquerque, NM, 1998.

[2] Knupp, P., and Salari, K., *Verification of Computer Codes in Computational Science and Engineering*, Chapman Hall/CRC Press, Boca Raton, FL, 2003.

[3] Sparrow, E. M., "Radiant Absorption Characteristics of Concave Cylindrical Surfaces," *Journal of Heat Transfer*, Vol. 84, 1962, pp. 283–293.

[4] Modest, M. F., *Radiative Heat Transfer*, 2nd ed., Academic Press, San Diego, CA, 2003.

[5] Sparrow, E. M., and Cess, R. D., *Radiation Heat Transfer*, Brooks/Cole, Belmont, CA, 1966.

[6] Siegel, R., and Howell, J. R., *Thermal Radiation Heat Transfer*, Taylor and Francis, New York, 2002.

[7] Mathews, J. H., *Numerical Methods for Mathematics, Science, and Engineering*, 2nd ed., Prentice–Hall, Englewood Cliffs, NJ, 1992.